IEEE Access
Multidisciplinary | Rapid Review | Open Access Journal

SPECIAL SECTION ON BIG DATA LEARNING AND DISCOVERY

Received August 15, 2018, accepted September 16, 2018, date of publication September 26, 2018, date of current version October 19, 2018.

Digital Object Identifier 10.1109/ACCESS.2018.2872168

Surface Saliency Detection Based on Curvature Co-Occurrence Histograms

NING WEI[1], KAIYUAN GAO[1], RONGRONG JI[2], AND PENG CHEN[1]
[1]College of Computer and Information Technology, China Three Gorges University, Yichang 443002, China
[2]School of Information Science and Engineering, Xiamen University, Xiamen 361005, China

Corresponding author: Peng Chen (chenpeng@ctgu.edu.cn)

This work was supported in part by the National Key Research and Development Program of China through the Ministry of Science and Technology of China under Grant 2016YFC0802500, in part by the Hubei Provincial Natural Science Foundation of China under Grant 2017CFB595, and in part by the National Natural Science Foundation of China under Grant 61871258 and Grant 61272236.

ABSTRACT This paper presents a 3-D surface saliency feature detection method, which can measure the importance geometry region of the point clouds. Different from existing approaches that are based on 3-D filter banks, the new method first constructs the curvature co-occurrence histogram (CCH), which encodes not only the global curvature occurrence, but also the co-occurrence of local distinctive features. And then, the mesh saliency is extracted from CCH through our mapping function. The proposed method is easy to implement and has high computation efficiency, which makes it especially suitable for large-scale 3-D point cloud preprocessing. The effectiveness of the saliency is demonstrated by point clouds' registration and mesh simplification. Experimental results, from visual and quantification, demonstrate that our saliency contains more local geometrical details information and has more stable globally measurement comparing with curvature only described feature and center-surround saliency.

INDEX TERMS Mesh saliency, mesh registration, mesh simplification, co-occurrence histogram.

I. INTRODUCTION

In recent years, with advances in high-speed 3D laser-scanning and depth range sensor technologies, the collected point clouds has higher density rate and also the scanned models have higher accuracy. Hence, most of the raw scanned models usually generate a huge amount of data points. It brings various challenges for storage, registration and transmission in real application. Thus, efficient and accurate simplification methods for the data are necessary. But the regions of mesh having relatively more important geometry features should be preserved. Therefore, measuring the importance is essential for preprocessing the mesh.

Pure geometric measures of mesh shape such as curvature have a long history of application in mesh processing literature. Such as simplification [1], smoothing [2], [3], shape matching [4], rending [5] and viewpoint selection [6]. However, a pure curvature-based metric may not necessarily be a good metric of perceptual importance [1]. For example, we elastically stretch a small part of a sphere mesh, as in Figure 1a, where the neck-like and bump region is likely perceived to be important. However, it is likely that the neck region has lower or equal curvature compared to the most bottom hemisphere region in Figure 1b. In the past years, visual saliency theory has been applied in the field of mesh feature detection. The salient regions can be used to detect the mesh vertices that are important for the 3D surface.

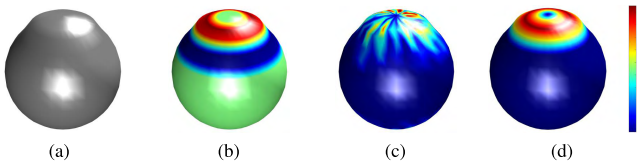

FIGURE 1. (a) Original mesh. (b) Shaded by Gauss curvature. (c) Lee [1] saliency. (d) Our saliency.

There has been a number of mesh feature detection methods which are based on visual saliency reported in recent years. These methods can be divided into local center-surround operator [7]–[10] and multi-scale computation [1], [2], [4], [11]. Leifman *et al.* [11] proposed a viewpoint selection method based on vertex distinctness. Gal and Cohen-Or [7] introduced a method for partial matching of surfaces represented by triangular meshes. Lee *et al.* [1] defined a center-surround operator on the local curvature as the discriminative feature. Pauly *et al.* [12] present a multi-scale technique for extracting surface variation and feature-points over different scales. And other local 3D shape

descriptor to extract the feature, such as [13] and [14]. These models are based only on the local feature operator. Hence, the error created during the curvature estimation will be amplified by the local difference operator, such as the saliency in Figure 1c which is detected by the center-surround model [1]. Zhao *et al.* [15] proposed a global model named shape index field based on non-local means filter, it runs very slowly especially for 3D point cloud.

In this paper, we present a novel mesh saliency model based on the curvature co-occurrence histogram (CCH). Analogously to co-occurrence histogram based image saliency detection method [16], [17], the proposed model concurrently encodes both global shape features occurrence and local discriminative shape features compared with the surroundings. Therefore, it can be determined based on the distinctive feature and common shape feature. Figure 1d is shaded by our proposed saliency, and it can be observed that the bump region is shaded in higher value than bottom hemisphere region, which is consistent with the visual perception. We can observe that the model is computationally fast and easy to be implemented. Hence, it is especially suitable for processing large data sets.

The effectiveness of the model is verified by point cloud registration and mesh simplification results. It demonstrates that our mesh saliency represent more important features than the state-of-the-art model.

II. ALGORITHM

The algorithm is highly related to the model proposed for image saliency model [16] and includes two phases. Firstly, it constructs the Curvature Co-occurrence Histogram, which not only is the statistic of the global curvature information but also the co-occurrence of curvature information in the local region. Secondly, the saliency for each mesh vertex is mapped from the CCH in our saliency model.

A. CURVATURE CO-OCCURRENCE HISTOGRAM CCH

Let $V = \{v_1, v_2 ... v_N\}$ is a point set in R^3 space. Its Gauss curvature denoted as $G = \{g(v_1), g(v_2), \cdots, g(v_N)\}$. Then we uniformly quantify the interval $[g_{min}, g_{max}]$ to $\mathbb{K} = \{1, 2, \cdots, k\}$ bins, i.e. k levels. We denote the quantified G as $\{g_1, g_2, \cdots, g_k\}$. The curvature co-occurrence histogram H is defined as:

$$H = [h(m, n)], \quad m, n \in \mathbb{K}, \tag{1}$$

where H is a symmetric square matrix of size $k \times k$. For each vertex v_i with a Gauss curvature g_i falls into m, all vertex within the neighborhood of v_i are examined one by one. If a neighboring vertex has a curvature value falls into n, the H element $h(m, n)$ is increased by one. H is built after all vertices of the model are examined. The neighborhood of the vertex v_i is defined as a ball centred at v_i with radius r denoted as $\mathcal{B}(v_i)^r$.

The CCH encodes both occurrence and co-occurrence of the vertices curvature. Each vertex pair with itself to account for many diagonal elements of the CCH, through which global shape occurrence information is captured. At the same time, each vertex pair with a number of neighborhood vertices, to account for non-diagonal elements of the CCH, through which local co-occurrence curvature feature is captured. For the Stanford bunny model in Figure 2a, Figure 2b shows its CCH.

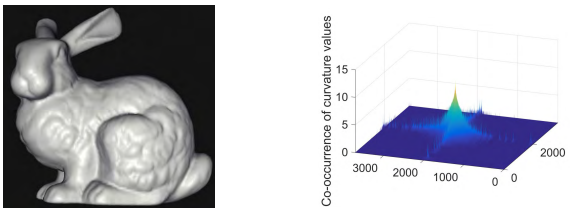

(a) (b)

FIGURE 2. (a) Original bunny model. (b) The curvature co-occurrence histogram of the bunny model. Since the Gauss curvature varies in a wide range, and some bins have large occurrence,we scale H as $\log(1 + H)$ for better visualization.

B. MESH SALIENCY FROM CCH

Mesh saliency is captured by two types of CCH elements. The first is that those elements far from the diagonal that correspond to small convex or concave parts of the mesh, such as eyes, foot in Figure 2a. The second is that those elements lying around the diagonal that correspond to mesh vertices paired with neighbors have relatively infrequent distribution, such as tail and ears in Figure 2b. We will establish a mapping from CCH to the vertex's saliency. We define a probability mass function (PMF) as:

$$P = \frac{H}{\sum_{m=1}^{k} \sum_{n=1}^{k} h(m, n)}. \tag{2}$$

The values in P are 0 or larger than the average should not be considered to be the contribution for saliency. And rest of the values are inversely proportional with saliency. The smaller probability value, the higher value of saliency. So an inverted $\bar{P}$ is computed as follows:

$$\bar{P} = \begin{cases} 0, & if\ P(m, n) = 0, \\ 0, & if\ P(m, n) > T, \\ T - P(m, n), & if\ P(m, n) \leq T, \end{cases} \tag{3}$$

where $p(m, n)$ denotes an element of P. As defined in (3), elements in $\bar{P}$ are set to 0 when there are no corresponding curvature value pairs within the model or when the corresponding P elements are lager than a certain threshold.

The threshold T in (3) is a measure of the average curvature value of model, which is set based on the average of nonzero elements within P as follows:

$$T = \frac{1}{\sum INZ(P)}, \tag{4}$$

where $INZ(P)$ denotes a binary nonzero function that sets all nonzero elements within P to 1 and rest to 0. The denominator $\sum INZ(P)$ counts all nonzero elements in P. As shown in Figure 2, the curvature value of the mouth is less than the threshold T, so it has great value in $\bar{P}$.

The salient value for each vertex v_i is computed as follows:

$$S(i) = \sum_{j \in \mathcal{B}(i)^r} \bar{P}(g_i, g_j), \tag{5}$$

where j index the vertices within the neighborhood of v_i, and r is set the same as in CCH construction. g_i and g_j denote curvature values at location v_i and v_j, respectively. Therefore, $\bar{P}(g_i, g_j)$ is the element of $\bar{P}$ indexed by g_i and g_j.

III. EXPERIMENTAL RESULTS

A. IMPLEMENTATION

There are 2 parameters need to be set in the algorithm. The first is the ball radius r which specifies the neighbor size of the given point. The second is the number of bins k involved in the curvature vectorization.

The CCH has a very good characteristic: It is tolerant to the variation of the radius r. To show that, we fix the parameter k to 3700 bins, and then set r as 2%,4%,6%,8% of the model diameter. Taking the bunny model as an example, we depict the same sampled row in CCH for each parameter of r. It shows in Figure 3 that the CCH is similar to each other under different r. The main difference is that when the radius r is much too smaller, the distribution of CCH is likely close to 0. This is because only fewer closest neighboring vertices having nearly same curvature are taken into statistics when the r is oversmall. Hence, the total energy of the CCH is too small and local discriminative geometry features can not be encoded properly.

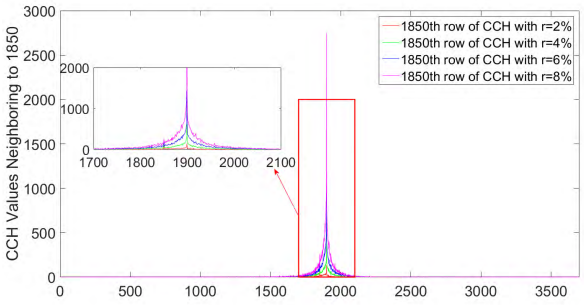

FIGURE 3. Comparison of the CCHs, which are calculated under different radius r. Each curve is got by sampling from a fixed row (1850th) of CCH.

Figure 4 shows the saliency of the bunny model under different radius $r = 2\%, 4\%, 6\%, 8\%$ of the model diameter. It can be seen that when r is greater than or equal to 4% of the model diameter, the saliency detection results have been slightly influenced by the parameter. Considering the efficiency of the algorithm, we set r equals to the 4% of the model diameter in this paper.

After the radius r is determined in the algorithm, we discuss how to confirm the size of the CCH, i.e. k. The complexity of the algorithm is highly relative to it. Firstly, we define N as the number of vertices on model. And then, the maximum computation time of (1), (2), (3), (4) and (5) are $\mathcal{T}(N^2)$, $\mathcal{T}(2k^2)$, $\mathcal{T}(k^2)$, $\mathcal{T}(k^2)$ and $\mathcal{T}(N^2)$, respectively. So the performance time of our algorithm is $\mathcal{T}(2N^2 + 4k^2)$.

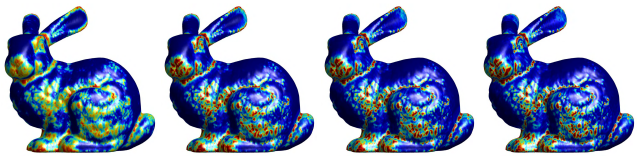

FIGURE 4. Salient feature detection results with different r. (a) r = 2%; (b) r = 4%; (c) r = 6%; (d) r = 8%.

In order to have a higher quantification level k but not to raise the complexity much, it is reasonable to set $k^2 \leq \frac{1}{2}N^2$. Although $k = (\frac{1}{2}N^2)^{\frac{1}{2}}$ gives higher quantification level, the CCH takes up too much storage space to compute. It would restrict the application scope of the CCH.

Therefore, we proposed a nonlinear function from that we have $k = (\frac{1}{2}N^2)^{\frac{2}{log_{10}N+1}}$. There are two main advantages of this function. Firstly, even for huge amount of point number N, the k is controlled in a computable scale, since it can be proofed that $\lim_{N \to +\infty} (\frac{1}{2}N^2)^{\frac{2}{log_{10}N+1}} = 10^4$ (The proof is represented in Appendix.). Secondly, in most case when N is got in the range from 10^5 to 10^6, the number of bins k has a moderate value in the range from 1710 to 2201.

Figure 5 plots the number of bins k varying with different number of vertices N. It shows that the bins number k increases slowly as the N increasing to infinity, and it is restricted under 10^4. Therefore, for any number of vertices of the model, the value k is satisfied with the limitations of computer hardware.

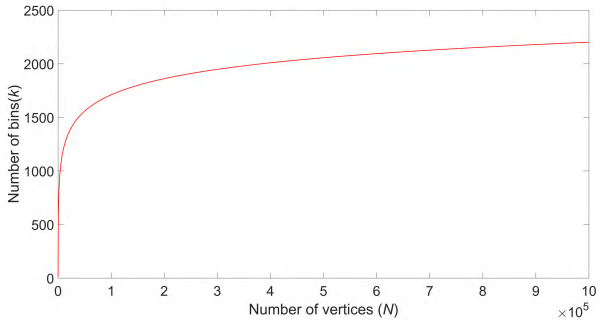

FIGURE 5. The number of bins k vary with different number of clouds scale N.

Figure 6 shows the saliency computed under different k. It shows that even set bigger quantification levels than our proposed k, the computed saliency has a slight variation. It is hard to conclude that the proposed k gives an optimal choice of quantification levels, but it get a balance between store space and accuracy.

In Table 1, we compare the computation time at different number of triangles. It can be seen that as the scale of point cloud increasing, the computation complexity increase extremely slower compares with the method in [1]. It makes our method extremely suitable for large scale point clouds feature detection.

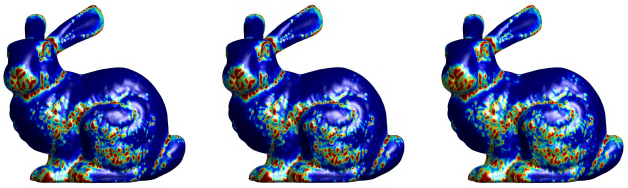

FIGURE 6. Salient feature detection results. The radius r is set to 4% of the model diameter and the number of vertices $N = 35947$. (a) $k = (\frac{1}{2}N^2)^{\frac{2}{\overline{log_{10}N+1}}} = 1485$; (b) $k = 5000$; (c) $k = 10000$.

TABLE 1. Computation efficiency comparison (sec).

Number of triangles	10k	20k	30k	40k	50k	60k
model in [1]	5.88	9.59	16.71	201.53	1450.91	13824.85
Ours	4.38	7.23	11.02	15.03	19.43	24.39

In Figure 1, we shaded the synthesized model using different detecting method. And our saliency is more consistent with the visual perception. Figure 7 presents the surface saliency for the model cow, bunny and dragon. It can be seen that the regions with more geometry information have been indicated with "warm colors".

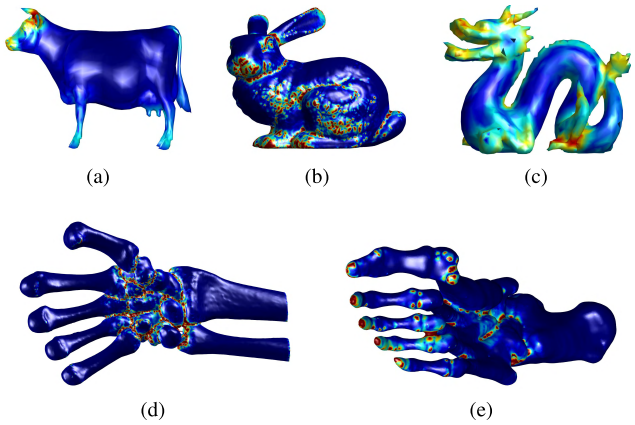

FIGURE 7. Salient feature detection results. The number of vertices N and bins k: (a) $N = 2904, k = 931$; (b) $N = 35947, k = 1485$; (c) $N = 2396, k = 890$; (d) $N = 72259, k = 1641$; (e) $N = 35406, k = 1484$.

Unlike in 2D images, 3D saliency detection does not have ground truth, so the accuracy of the detected saliency cannot be determined. To solve this problem, point cloud registration and mesh simplification approach is applied. The simplification and registration errors indicate the efficiency of the proposed saliency detection method. According to the points' saliency value, we can sample faithful points in registration, and exert weight on important vertices to preserve the local geometrical details in simplification. Figure 8c shows the sampled points which are obtained by our saliency. Higher salient regions will have more sampling points. Figure 8d shows the 95% simplified mesh, and the details is presented in III-C.

B. REGISTRATION

In this paper, the ICP algorithm [18], [19] is used for registering the sampled points. For an original point cloud V in $\mathbb{R}^3$,

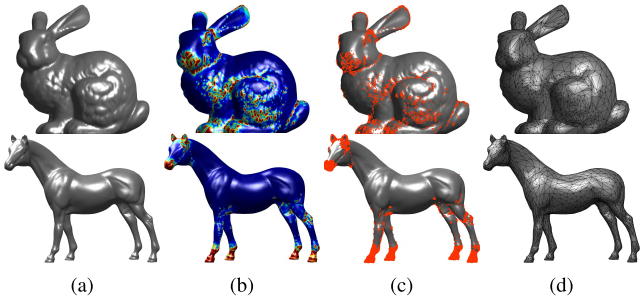

FIGURE 8. (a) Input model bunny and horse. (b) Our saliency. (c) Selected salient points, 10% were selected. (d) 95% simplified model.

and the source point cloud V' can be computed as:

$$V' = R_\theta \cdot D(V), \tag{6}$$

Where $D(\cdot)$ denotes downsampling point cloud V according to the points' salient value. R is the rotation matrix and the rotation parameter θ is set to 20°. We fix the point cloud V as the target and estimate $R_{\theta'}$ to register V' to V. The ICP algorithm iteratively converge to the final estimation parameter $R_{\theta'}$, which can minimize the distance of point set V and V'.

The efficiency of the saliency detection can be eventually determined by the registered RMSE (root mean square error) $|V - V'| = \sqrt{\sum_{v'_i \in V'}(v_i - v'_i)^2}$ and $\Delta\theta = |\theta - \hat{\theta}|$. Usually, the RMSE and angle estimating error indicate the performance of the algorithm. Figure 9 shows the ICP registration results as the subsampling rate P varying from 50% to 90%. It can be observed that the proposed method achieves comparable accuracy with [1] under RMSE criteria, while our method has relatively better results for θ estimation.

C. SIMPLIFICATION

In order to evaluate the effect of the simplification efficiency, our simplification results have been compared with QEM (Geometric quadric error metrics) method [20] and Lee-QEM (Lee saliency weighted QEM) method [1]. Analogous to Lee-QEM, we use the salient feature as the weight and exert

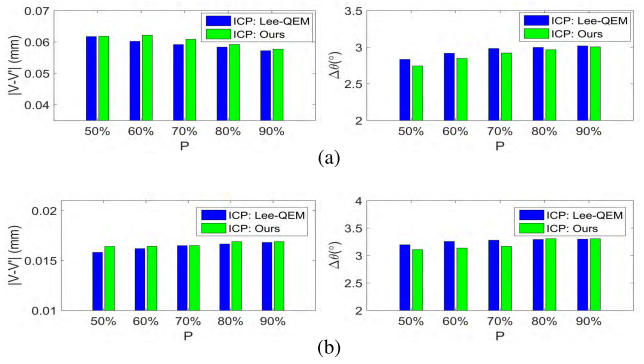

FIGURE 9. The ICP registration results based on our method and Lee-QEM [1]. Applied on cow and bunny with 20° rotation angle, respectively. First column: the RMSE error of registration. Second column: the error of estimated rotation angle $\Delta\theta$. P is the percentage that sampled from the original point cloud. (a) Cow. (b) Bunny.

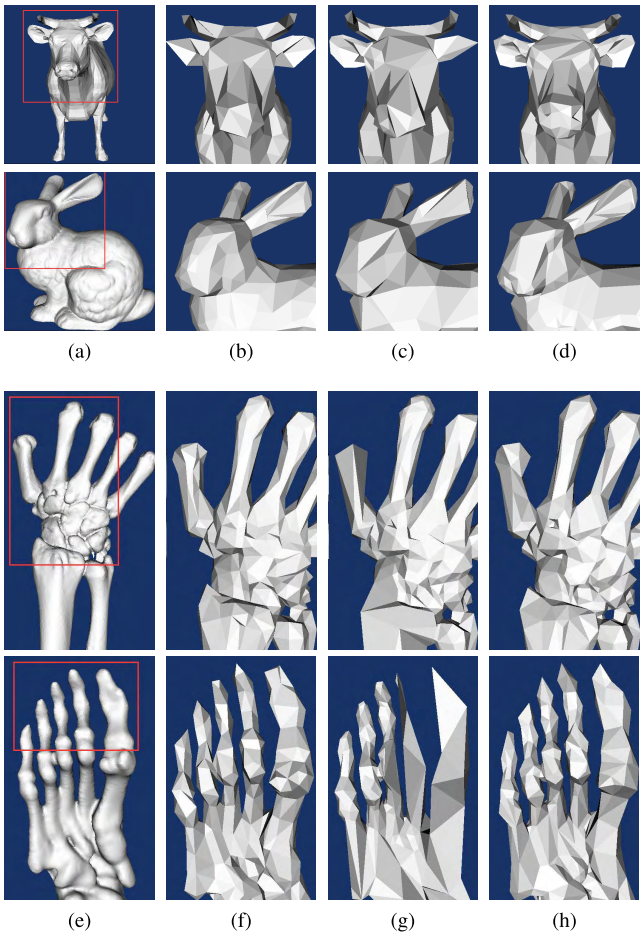

FIGURE 10. Simplify by using QEM [20], Lee-QEM [1] and our method to 1k triangles. (a)(e) Original models (cow has 5804 triangles, bunny has 69451 triangles, wrist has 141232 triangles and feet has 70368 triangles. (b)(f) QEM [20]. (c)(g) Lee-QEM [1]. (d)(h) Ours.

it to mesh vertices during simplification. At the initialization, the quadric matrix Q for each vertex v is multiplied by its simplification weight W derived from the saliency of v: $Q \leftarrow W(v)Q$. After a vertex-pair collapse, the weight W for the new vertex is the sum of the weight for the pair of vertices being collapsed $W(v_i)+W(v_j)$. The weight for vertex is defined as:

$$W(v) = \begin{cases} \lambda S(v_i), & if\ S(v_i) \geq \alpha, \\ S(v_i), & if\ S(v_i) < \alpha, \end{cases} \tag{7}$$

where $W(\cdot)$ amplifies the salient value by λ to those salient value bigger than a threshold α. This will ensure that the important salient vertices will preserve their position longer. In our method and Lee-QEM [1], we all set $\lambda = 100$ and $\alpha = 30\%$ percentile saliency.

Figure 10 shows the visual quality comparison of the three simplification methods. We simplify each model to 1k triangles from the original models. Apparently, our method for all models even for 3D medical models which was generated from CT scan in retaining local details is much better than the QEM and Lee-QEM. Our method preserves the shapes

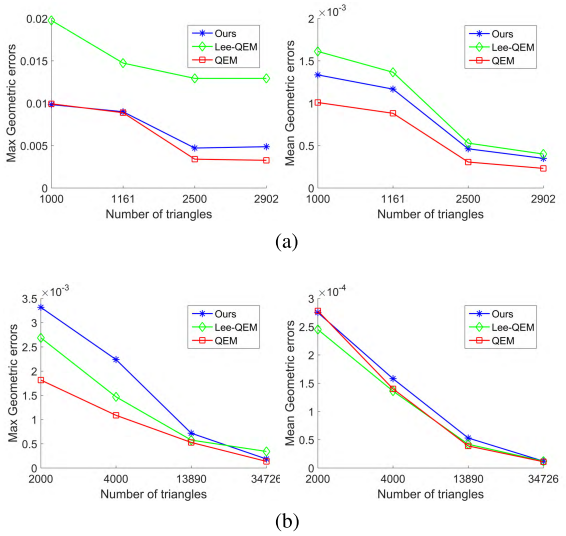

FIGURE 11. Metro [21] to evaluate the geometric errors. First column: Max geometric errors. Second column: Mean geometric errors. (a) Cow. (b) Bunny.

of noses and mouths better. Other methods result in blurring or distortion in these regions.

To quantificationally compare the simplified results, we use triangular mesh error evaluation software Metro [21], which can measure the difference between the original model and simplified model. The Max geometric errors and mean geometric errors of the three methods are showed in Figure 11. It can be observed that our method has a moderate performance under both types of error criterion. We can deduce that our saliency not only gives an accurate measure for the salient surface region but also conduct properly at the non-salient region, which means that our saliency has a stable measure for mesh globally.

IV. CONCLUSION

In this paper, we have presented a novel 3D surface saliency detection method, which makes use of curvature co-occurrence histograms. Compared with state-of-the-art models, the proposed model has a high efficiency in computation especially suitable for large-scale date set processing. The registration results show that the points sampled from our saliency capture the main geometry features of the model. Therefore registering using points extracted from our saliency and points from other saliency have almost same registration error. The performances of simplification on various data show that our approach not only represents overall shape fidelity but also has the capability to retain the sharp and visual salient regions well.

APPENDIX
PROOF THE UPPER BOUND OF THE PROPOSED QUANTIFICATION LEVELS *k*

$$\lim_{N \to +\infty} (\frac{1}{2}N^2)^{\frac{2}{log_{10}N+1}} = 10^4$$

Proof:

$$\begin{aligned}\lim_{N\to+\infty}\left(\frac{1}{2}N^2\right)^{\frac{2}{log_{10}N+1}} &= e^{\lim_{N\to+\infty}\frac{2}{log_{10}N+1}\cdot\ln\frac{1}{2}N^2}\\ &= e^{\lim_{N\to+\infty}\frac{2\ln\frac{1}{2}N^2}{\frac{\ln N}{\ln 10}+1}}\\ &= e^{\lim_{N\to+\infty}\frac{4\ln N+2\ln\frac{1}{2}}{\ln N+\ln 10}\cdot\ln 10}\\ &= e^{4\ln 10}\\ &= 10^4\end{aligned}$$

REFERENCES

[1] C. H. Lee, A. Varshney, and D. W. Jacobs, "Mesh saliency," *ACM Trans. Graph.*, vol. 24, no. 3, pp. 659–666, Jul. 2005.

[2] J. Wu, X. Shen, W. Zhu, and L. Liu, "Mesh saliency with global rarity," *Graph. Models*, vol. 75, no. 5, pp. 255–264, 2013.

[3] C. Lange and K. Polthier, "Anisotropic smoothing of point sets," *Comput. Aided Geometric Des.*, vol. 22, no. 7, pp. 680–692, 2005.

[4] P. Shilane and T. Funkhouser, "Distinctive regions of 3D surfaces," *ACM Trans. Graph.*, vol. 26, no. 2, 2007, Art. no. 7.

[5] H. Yee, S. Pattanaik, and D. P. Greenberg, "Spatiotemporal sensitivity and visual attention for efficient rendering of dynamic environments," *ACM Trans. Graph.*, vol. 20, no. 1, pp. 39–65, Jan. 2001.

[6] M. Feixas, M. Sbert, and F. González, "A unified information-theoretic framework for viewpoint selection and mesh saliency," *ACM Trans. Appl. Perception*, vol. 6, no. 1, 2009, Art. no. 1.

[7] R. Gal and D. Cohen-Or, "Salient geometric features for partial shape matching and similarity," *ACM Trans. Graph.*, vol. 25, no. 1, pp. 130–150, Jan. 2006.

[8] X. Li and I. Guskov, "Multiscale features for approximate alignment of point-based surfaces," in *Proc. Symp. Geometry Process.*, vol. 255, 2005, pp. 217–226.

[9] N. Gelfand, N. J. Mitra, L. J. Guibas, and H. Pottmann, "Robust global registration," in *Proc. Symp. Geometry Process.*, 2005, Art. no. 197.

[10] Y. Kim, A. Varshney, D. W. Jacobs, and F. Guimbretière, "Mesh saliency and human eye fixations," *ACM Trans. Appl. Perception*, vol. 7, no. 2, 2010, Art. no. 12.

[11] G. Leifman, E. Shtrom, and A. Tal, "Surface regions of interest for viewpoint selection," in *Proc. IEEE Conf. Comput. Vis. Pattern Recognit. (CVPR)*, Jun. 2012, pp. 414–421.

[12] M. Pauly, R. Keiser, and M. Gross, "Multi-scale feature extraction on point-sampled surfaces," *Comput. Graph. Forum*, vol. 22, no. 3, pp. 281–289, Sep. 2003.

[13] Y.-L. Yang and C.-H. Shen, "Multi-scale salient feature extraction on mesh models," in *Proc. Int. Conf. Comput. Vis. Media*. New York, NY, USA: Springer-Verlag, 2012, pp. 122–129.

[14] Y. Lei, M. Bennamoun, M. Hayat, and Y. Guo, "An efficient 3D face recognition approach using local geometrical signatures," *Pattern Recognit.*, vol. 47, no. 2, pp. 509–524, Feb. 2014.

[15] Y. Zhao, Y. Liu, R. Song, and M. Zhang, "Extended non-local means filter for surface saliency detection," in *Proc. 19th IEEE Int. Conf. Image Process. (ICIP)*, Sep./Oct. 2012, pp. 633–636.

[16] S. Lu, C. Tan, and J.-H. Lim, "Robust and efficient saliency modeling from image co-occurrence histograms," *IEEE Trans. Pattern Anal. Mach. Intell.*, vol. 36, no. 1, pp. 195–201, Jan. 2014.

[17] L. Zhang and A. Li, "Region-of-interest extraction based on saliency analysis of co-occurrence histogram in high spatial resolution remote sensing images," *IEEE J. Sel. Topics Appl. Earth Observat. Remote Sens.*, vol. 8, no. 5, pp. 2111–2124, May 2015.

[18] P. J. Besl and N. D. McKay, "A method for registration of 3-D shapes," *IEEE Trans. Pattern Anal. Mach. Intell.*, vol. 14, no. 2, pp. 239–256, Feb. 1992.

[19] Y. Chen and G. Medioni, "Object modelling by registration of multiple range images," *Image Vis. Comput.*, vol. 10, no. 3, pp. 145–155, Apr. 1992.

[20] M. Garland and P. S. Heckbert, "Surface simplification using quadric error metrics," in *Proc. 24th Annu. Conf. Comput. Graph. Interact. Techn.* Reading, MA, USA: Addison-Wesley, 1997, pp. 209–216.

[21] P. Cignoni, C. Rocchini, and R. Scopigno, "*Metro*: Measuring error on simplified surfaces," *Comput. Graph. Forum*, vol. 17, no. 2, pp. 167–174, 1998.

NING WEI received the Ph.D. degree from the School of Information Science and Engineering, Lanzhou University, China, in 2010. He is currently an Associate Professor with the College of Computer and Information Technology, China Three Gorges University, Yichang, China. His research interests include computer vision, pattern recognition, and computer graphics.

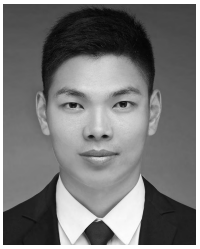

KAIYUAN GAO was born in Yichang, Hubei, China, in 1992. He received the master's degree from the College of Computer and Information Technology, China Three Gorges University, Yichang. His main research interests are image processing and mesh simplification.

RONGRONG JI received the Ph.D. degree in computer science from the Harbin Institute of Technology, China. He has been a Post-Doctoral Researcher along with Prof. S.-F. Chang at Columbia University since 2011.He was a Research Assistant along with Prof. Wen Gao at Peking University, was a Research Intern along with Dr. Wei-Ying Ma at Microsoft Research Asia, and had led the Visual Intelligence Laboratory, Multimedia Retrieval Group, Harbin Institute of Technology, from 2007 to 2010. He has authored over 25 tier-1 conferences, including CVPR, ACM Multimedia, IJCAI, and AAAI, and over 10 IEEE/ACM TRANSACTIONS and IJCV. His research interests include image and video search, scene parsing, and large-scale object recognition. He was a recipient of the Best Paper Award at the ACM Multimedia 2011 and the Microsoft Fellowship 2007. He is the leading Guest Editor for *IEEE Multimedia Magazine*, an Associate Editor for frontiers in computer science, and the Special Session Chairs for VCIP 2013, PCM 2012, MMM 2012, ICIMCS 2012 and 2010, and ICME 2008. He has served as a Technical Program Committee Member in over 40 international conferences including CVPR, ICCV, ECCV, and ACM Multimedia, and over 10 IEEE/ACM TRANSACTIONS.

PENG CHEN was born in Enshi, Hubei, China, in 1973. He received the B.S. and M.S. degrees from Huazhong Normal University and the Ph.D. degree in system analysis and integration from the Huazhong University of Science and Technology. From 2005 to 2011, he was a Senior Engineer with the Information Technology Center, China Three Gorges University. Since 2012, he has been a Professor with the Computer and Information Institute, China Three Gorges University. He has authored one book and over 50 articles. His research interests include computer graphics, augmented reality, parallel computing, and big data.